IEEE Access
Multidisciplinary | Rapid Review | Open Access Journal

Received August 18, 2021, accepted August 30, 2021, date of publication September 1, 2021, date of current version September 10, 2021.

Digital Object Identifier 10.1109/ACCESS.2021.3109587

Decoupling of Isosceles Triangular Array by Loaded Parasitic Element in Combination With Decoupling and Matching Network

CHI ZHANG, (Member, IEEE), YONG-CHANG JIAO, (Senior Member, IEEE), JINGXUAN WEN, YANG-DONG YAN, AND ZIBIN WENG, (Senior Member, IEEE)
National Key Laboratory of Antennas and Microwave Technology, Xidian University, Xi'an 710071, China

Corresponding author: Zibin Weng (zibinweng@mail.xidian.edu.cn)

This work was supported by the National Square Kilometre Array (SKA) Program of China under Grant 2020SKA0110300.

ABSTRACT In this paper, decoupling of a compact isosceles triangular array is performed by a hybrid method consisting of loaded parasitic element (LPE) in combination with decoupling and matching network (DMN). By introducing a reactively loaded parasitic element at a suitable position on the axis of symmetry of the isosceles triangle, not only are the mutual couplings between the element at the vertex and the two elements on the base eliminated but also the circuit parameters of the base elements are well prepared for a DMN of a simpler form. Thus, the impedance matching of the vertex element and the decoupling and matching of the base elements can be implemented independently. The DMN of base elements comprises two impedance-transforming sections (ITS) and a π-shaped neutralization section (NS). The ITSs inserted between the antennas and NS convert the self-conductance to the system admittance and the trans-conductance to zero. The trans-susceptance is then compensated through the main line of the NS independently, and self-susceptance is canceled out by adjusting the tapped stubs subsequently. With all the explicit formulas derived, the design is systematic and straightforward. The presented compact isosceles triangular array with element separations of 0.1λ and 0.2λ is fabricated and measured. The results show that sound isolation of 35 dB and return loss of 21 dB is obtained with ECCs less than 0.02, validating the effectiveness of the hybrid decoupling technique.

INDEX TERMS Decoupling and matching network, mutual coupling, parasitic element, triangular array.

I. INTRODUCTION

Multiple-input multiple-output (MIMO) technology adds signaling dimensions across multiple antennas, enhancing the channel capacity within the limited bandwidth and power levels [1]. Consequently, it grew into a foundation of wireless communication systems [2]. However, to follow the trend towards compact terminals, multiple antennas are forced to occupy a small footprint, resulting in undesired mutual couplings [3]. Due to the strong coupling, the high signal correlations and efficiency reduction will significantly degrade the system performance.

The past two decades have seen increasingly advances in the field of mutual coupling reduction. Despite the relatively narrow bandwidth of various existing decoupling methods, integrating electronically tunable antenna technologies [4] makes these methods more practical. The electromagnetic band-gap (EBG) structure with an equivalent circuit of LC parallel resonator [5] is proposed to alleviate mutual coupling by suppressing the propagation of surface wave [6], but the large size violates the original intention of miniaturization. In [7] and [8], the defected ground structures (DGS) act as a band-stop filter utilizing a shorted $\lambda/4$ resonator. The ground current flowing routine is disturbed, which results in a reduction of mutual coupling. Although the decoupling effect is appealing, etching on the ground is not conducive to the integration with the system. Another method involving ground modification is protruding the ground to form an additional resonator [9]–[12]. The coupling from the new path through the resonator cancels out the modified existing one; thus, high isolation can be obtained. Neutralization lines inserted between two radiators have the exact mechanism

The associate editor coordinating the review of this manuscript and approving it for publication was Qi Luo.

as the above method [13], [14]. Without clear guidance, the structural variables involved have high degrees of freedom leading to a time-consuming EM optimization.

The methods that can be applied to various antenna types without changing the original antenna structure are the reactive loaded parasitic element (LPE)[15]–[19] and decoupling networks [20]–[31]. How the trans-parameter of two radiators varies with the load connected to the parasitic scatter is analyzed and formulated [15]. Under this rigorous criterion, an optimal decoupling solution can be obtained easily by a simple EM parameter sweeping. Eigenmode decomposition networks [20]–[22] employing rat-race couplers are investigated to separates two orthogonal modes of coupled antennas. The differential mode with opposite-phase currents on the two closely spaced radiators is intrinsically connected to a minimal impedance bandwidth. If the sum and differential patterns are not needed, choosing the multiport conjugate network [21]–[30] with a broader bandwidth can be better. A pair of impedance transforming sections (ITS), which may be realized by a lumped element or transmission line (TL), are cascaded to convert the trans-admittance to a purely imaginary number. Then a lossless neutralization section (NS) with pure imaginary admittance parameters is attached to cancel out the trans-admittance. When a lumped element is used as an NS [23], [24], it is difficult to find an element with the exact value calculated, which reduces the decoupling performance. In [26], a decoupling and matching network (DMN) is demonstrated, whose stub-loaded TL satisfies both the decoupling and matching conditions. Using a pair of coupled resonators as an NS can broaden the decoupling bandwidth [27], [28], but the disadvantage is that it increases the circuit area and design complexity.

The above two methods replace time-consuming EM optimization with circuit design under closed formulas, which determines that they are suitable to be extended to the decoupling of multi-element arrays. Nevertheless, as the number of array elements increases, their design complexity will inevitably increase. Circuit parameter matrices of a uniform three-element array are circulant and symmetric. Taking advantage of this rotational symmetry, if the loaded parasitic element method is utilized for decoupling, only one parasitic element is sufficient [15]. The decoupling networks also work, but the occupied area is slightly larger [28], [30], [31].

However, when a three-element array has only one axis of symmetry, which can be a linear array or isosceles triangular array, the analysis and design of the decoupling network will become more complicated. Experimentally verified decoupling networks for an isosceles triangular array are not available. A solution to a linear three-element array has been demonstrated, whose limitation is that the spacing between the nonadjacent elements should be $\lambda/4$ [29]. Turn to the LPE method; two parasitic elements are carried out to reduce mutual couplings of a three-element linear array [17]. The coupling of the two elements on the side differs from the coupling between the center element and the element on the side; therefore, EM optimizations are involved. One parasitic element can also decouple the isosceles triangular array by optimizations [18], but the isolation enhancement is limited, i.e., the farther the vertex angle differs from 60°, the worse the enhancement. Although the calculation-based parasitic element method [19] is not restricted by the array arrangement, avoiding time-consuming optimizations simultaneously, three parasitic elements are inserted to deal with the couplings resulting in a complexity of assembly.

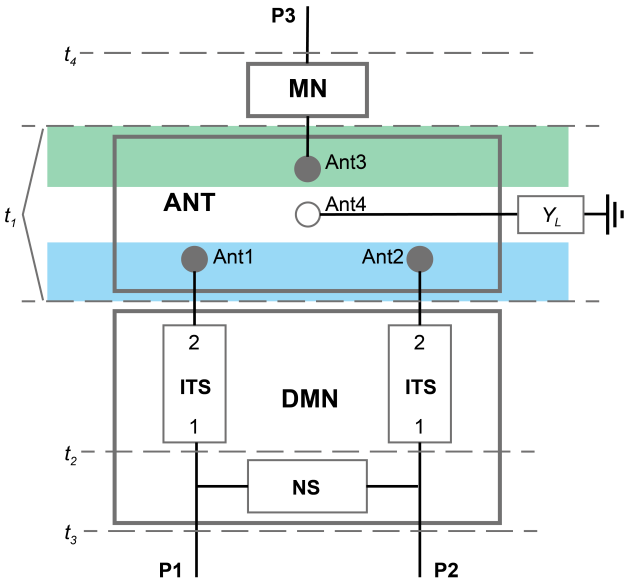

FIGURE 1. Diagram of the proposed hybrid decoupling technique.

A hybrid method consisting of loaded parasitic element (LPE) and decoupling and matching network (DMN) is presented to reduce the mutual couplings of a compact isosceles triangular array. Only one parasitic element is introduced by a simple EM parameter sweeping to decouple the vertex element from the other two elements. Besides, the circuit parameters of the base elements are transformed to satisfy a more straightforward design of the subsequent DMN simultaneously. Compared with the traditional stub-loaded DMN [26], the proposed DMN decouples the decoupling and matching conditions; hence, the compensation of the trans- and self- susceptance can be performed step by step. This decoupling scheme involves the least number of parasitic elements and avoids complex circuit analysis, which is systematic and straightforward.

The remainder of this paper is organized as follows. In Section II, the hybrid LPE–DMN method is described with theoretical derivations. Section III present a design example of a closely spaced isosceles triangle array, which is experimentally verified in Section IV. Conclusions are given in Section V.

II. HYBRID DECOUPLING TECHNIQUE

A. INTRODUCING LOADED PARASITIC ELEMENT

As shown in Fig. 1, the symmetry of the network parameters of the isosceles triangular array is that: the self-impedance/admittances of the two elements (Ant1 and 2)

at the bottom side are the same, and the mutual impedance/admittances of the vertex element (Ant3) and two base elements are the same. Introducing a loaded parasitic element (Ant4) on the axis can remove the coupling either between the base elements or between the vertex and base elements. The required parasitic element sizes and loading reactance values for decoupling two types of couplings are different. Thus, the method presented in [18] is a trade-off between removing these two types of coupling. Consequently, the effect of overall decoupling is restricted. Moreover, the isolation will get worse after the impedance matching is performed. We choose to remove only the coupling between the vertex element and the base elements to get an optimal solution. Because the decoupling effect of the LPE method is excellent, the isolation can reach more than 40dB at the reference plane t_1. Thus, the triangular array can be treated as two independent parts: the isolated vertex element (green region) and the compact two-element array with mutual coupling (blue region).

The circuit analysis by admittance [18] or impedance parameters [15] is equivalent. In order to facilitate subsequent discussions on the DMN, admittance parameters are selected here. The four-port network parameters after the introduction of the parasitic element on the axis can be described as

$$\boldsymbol{Y^A} = \begin{bmatrix} Y_{11}^A & Y_{12}^A & Y_{13}^A & Y_{14}^A \\ Y_{12}^A & Y_{11}^A & Y_{13}^A & Y_{14}^A \\ Y_{13}^A & Y_{13}^A & Y_{33}^A & Y_{34}^A \\ Y_{14}^A & Y_{14}^A & Y_{34}^A & Y_{44}^A \end{bmatrix} \tag{1}$$

The current-voltage relation at the port of the parasitic element with a load of Y_L is expressed by

$$I_4 = Y_L V_4 \tag{2}$$

Substituting (2) into (1) yields the admittance matrix across the ports of the three active elements at the reference plane t_1 as

$$\boldsymbol{Y^{t_1}} = \begin{bmatrix} Y_{11}^{t_1} & Y_{12}^{t_1} & Y_{13}^{t_1} \\ Y_{12}^{t_1} & Y_{11}^{t_1} & Y_{13}^{t_1} \\ Y_{13}^{t_1} & Y_{13}^{t_1} & Y_{33}^{t_1} \end{bmatrix} \tag{3}$$

where

$$\begin{aligned} Y_{11}^{t_1} &= Y_{11}^A - \frac{Y_{14}^{A^2}}{Y_L + Y_{44}^A} \\ Y_{33}^{t_1} &= Y_{33}^A - \frac{Y_{34}^{A^2}}{Y_L + Y_{44}^A} \\ Y_{12}^{t_1} &= Y_{12}^A - \frac{Y_{14}^{A^2}}{Y_L + Y_{44}^A} \\ Y_{13}^{t_1} &= Y_{13}^A - \frac{Y_{14}^A Y_{34}^A}{Y_L + Y_{44}^A} \end{aligned} \tag{4}$$

Decoupling the vertex element from the base elements requires $Y_{13}^{t_1} = 0$, whose solution is expressed as

$$Y_L = \frac{Y_{14}^A Y_{34}^A}{Y_{13}^A} - Y_{44}^A \tag{5}$$

In cases of a given position of LPE, a pure imaginary load can be obtained by a parameter sweeping of the element's length, which minimizes the ohmic loss introduced by the LPE.

Subsequently, an optimal decoupling is achieved, leaving the isolated vertex element (green region) and the compact two-element array with mutual coupling (blue region). Substituting (5) into (4), the admittance of green region is reduced as

$$Y^G = Y_{33}^{t_1} = Y_{33}^A - \frac{Y_{13}^A Y_{34}^A}{Y_{14}^A} \tag{6}$$

In addition, the admittance matrix of the two-port blue region is derived as

$$\boldsymbol{Y^B} = \begin{bmatrix} Y_{11}^B & Y_{12}^B \\ Y_{12}^B & Y_{11}^B \end{bmatrix} \tag{7}$$

where

$$\begin{aligned} Y_{11}^B &= Y_{11}^{t_1} = Y_{11}^A - \frac{Y_{13}^A Y_{14}^A}{Y_{34}^A} \\ Y_{12}^B &= Y_{12}^{t_1} = Y_{12}^A - \frac{Y_{13}^A Y_{14}^A}{Y_{34}^A} \end{aligned} \tag{8}$$

B. LOADED PARASITIC ELEMENT AND IMPEDANCE TRANSFORMING SECTION

The DMN is composed of two impedance transformation sections (ITS) and a neutralization section (NS). At the reference plane t_3, the decoupling and matching of the two ports should be satisfied, which can be described as

$$\begin{aligned} \boldsymbol{Y^{t_3}} &= \boldsymbol{Y^{t_2}} + \boldsymbol{Y^N} \\ &= \begin{bmatrix} Y_{11}^{t_2} + Y_{11}^N & Y_{12}^{t_2} + Y_{12}^N \\ Y_{12}^{t_2} + Y_{12}^N & Y_{11}^{t_2} + Y_{11}^N \end{bmatrix} = \begin{bmatrix} Y_0 & 0 \\ 0 & Y_0 \end{bmatrix} \end{aligned} \tag{9}$$

Because the entries in the admittance matrix of a lossless NS are pure imaginary, equation (9) demands that ITSs convert the real part of Y_{11} to the source conductance Y_0, and the real part of Y_{12} to zero at the reference plane t_2, i.e.,

$$\begin{aligned} \Re\left\{Y_{11}^{t_2}\right\} &= Y_0 \\ \Re\left\{Y_{12}^{t_2}\right\} &= 0 \end{aligned} \tag{10}$$

The ABCD matrix of the blue region can be transformed from the admittance matrix as

$$\boldsymbol{A^B} = -\frac{1}{Y_{12}^B} \begin{bmatrix} Y_{11}^B & 1 \\ \left|\boldsymbol{Y^B}\right| & Y_{11}^B \end{bmatrix} \tag{11}$$

where $\left|\boldsymbol{Y^B}\right|$ denotes the determinant of $\boldsymbol{Y^B}$. Then cascading the ITSs and the two-port network in the blue region yields

the ABCD matrix at t_2 as

$$\boldsymbol{A^{t_2}} = -\frac{1}{Y_{12}^B}\begin{bmatrix} A^I & B^I \\ C^I & D^I \end{bmatrix}\begin{bmatrix} Y_{11}^B & 1 \\ |\boldsymbol{Y^B}| & Y_{11}^B \end{bmatrix}\begin{bmatrix} D^I & B^I \\ C^I & A^I \end{bmatrix} \quad (12)$$

After an ABCD-to-Y transformation, we obtain

$$Y_{11}^{t_2} = \frac{A^I C^I + B^I D^I + Y_{11}^B (A^I D^I + B^I C^I)}{A^{I^2} + B^{I^2}|\boldsymbol{Y^B}| + 2A^I B^I Y_{11}^B}$$
$$Y_{11}^{t_2} = \frac{Y_{12}^B}{A^{I^2} + B^{I^2}|\boldsymbol{Y^B}| + 2A^I B^I Y_{11}^B} \quad (13)$$

To simplify the analysis, the ITS is chosen as a symmetric, lossless, and reciprocal network with the following form

$$\boldsymbol{A^I} = \begin{bmatrix} \alpha\beta & j\beta \\ j\dfrac{1-(\alpha\beta)^2}{\beta} & \alpha\beta \end{bmatrix} \quad (14)$$

where α, β are real. Substituting (14) into (13) in combination with (10) yields

$$\alpha_i = \frac{G_{12}^B B_{11}^B - G_{11}^B B_{12}^B + (-1)^{\left\lceil \frac{i}{2} \right\rceil} |Y_{12}^B| \sqrt{G_{11}^{B^2} - G_{12}^{B^2}}}{G_{12}^B}$$
$$\beta_i = (-1)^i \sqrt{\frac{G_{11}^B |Y_{12}^B| + (-1)^{\left\lceil \frac{i}{2} \right\rceil} |B_{12}^B| \sqrt{G_{11}^{B\,2} - G_{12}^{B_2}}}{2Y_0 |Y_{12}^B| \left(G_{11}^{B\,2} + B_{12}^{B\,2}\right)}} \quad (15)$$

where $i = 1, 2, 3, 4$. When we choose a transmission line (TL) of characteristic impedance Z and electrical length θ as the NS, the solutions are given as follows

$$Z^I = \frac{|\beta|}{\sqrt{1-(\alpha\beta)^2}}$$
$$\theta^I = arccos\,(\alpha\beta) \quad (16)$$

where

$$\alpha_{1,2} = \frac{G_{12}^B B_{11}^B - G_{11}^B B_{12}^B \pm |Y_{12}^B| \sqrt{G_{11}^{B\,2} - G_{12}^{B^2}}}{G_{12}^B}$$
$$\beta_{1,2} = \sqrt{\frac{G_{11}^B |Y_{12}^B| \pm |B_{12}^B| \sqrt{G_{11}^{B\,2} - G_{12}^{B^2}}}{2Y_0 |Y_{12}^B| \left(G_{11}^{B\,2} + B_{12}^{B\,2}\right)}} \quad (17)$$

Here omit two solutions with the electrical lengths greater than π.

According to the closed formulas above, the ITS design parameters can be calculated when an exact position of the parasitic element is given. Thus, we can alter the position of the LPE to obtain an ITS with parameters that are most convenient for implementation and adjustment.

C. NEUTRALIZATION SECTION

The proposed π-shaped TL is demonstrated in Fig. 2 (a), which is composed of a TL with a characteristic admittance of Y_1^N and electrical length of θ_1^N, and two identical shunt load of jB_L^N connected to the ends.

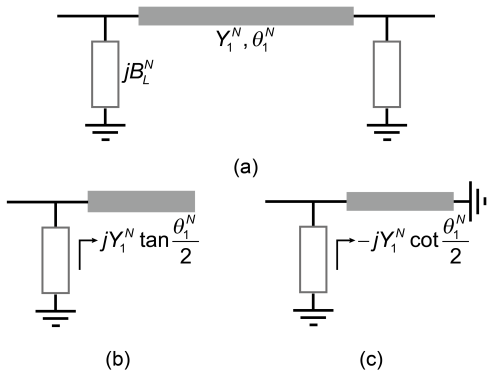

FIGURE 2. (a) Equivalent structure of the proposed neutralization section. (b) Even-mode and (c) odd-mode circuits.

Applying the even-odd method to the NS, the even and odd equivalent circuits are shown in Fig. 2 (b) and (c). Thus, the even and odd admittances are given by

$$Y_e^N = jY_1^N tan\left(\frac{\theta_1^N}{2}\right) + Y_L^N$$
$$Y_o^N = -jY_1^N cot\left(\frac{\theta_1^N}{2}\right) + Y_L^N \quad (18)$$

By the definitions of even and odd admittances, the entries in the admittance of the NS can be derived as

$$Y_{11}^N = \frac{Y_e^N + Y_o^N}{2} = -jY_1^N cot\theta_1^N + jB_L^N$$
$$Y_{12}^N = \frac{Y_e^N - Y_o^N}{2} = jY_1^N csc\theta_1^N \quad (19)$$

The function of the NS is compensating the self- and trans-susceptances at the references plane t_3. From (9), the decoupling and matching conditions are reduced to

$$Y_1^N csc\theta_1^N = -\Im\left\{Y_{12}^{t_2}\right\} \quad (20)$$
$$B_L^N = Y_1^N cot\theta_1^N - \Im\left\{Y_{11}^{t_2}\right\} \quad (21)$$

It can be seen that only the mainline contribute to the decoupling condition, i.e., (20), suggesting that decoupling should be implemented prior to the matching. Thus, adjusting the jB_L^N has no impact on the mutual coupling, which facilitates the neutralization compared with the existing method [26].

D. DESIGN PROCEDURES

The design procedures are summarized as follows:

(1) Insert the parasitic monopole at a given position on the axis, and then adjust the length of it to make the real part of Y_L calculated by (5) equal to zero at the center frequency.
(2) Calculate the admittance parameters at plane t_1, i.e., Y^G and $\boldsymbol{Y^B}$, by (6) and (8). The parameters of corresponding ITS can be obtained by (16) and (17).
(3) Alter the position of the LPE, and return to step 1 for several times to obtain a position where the parameters of the ITS are convenient for implementation.

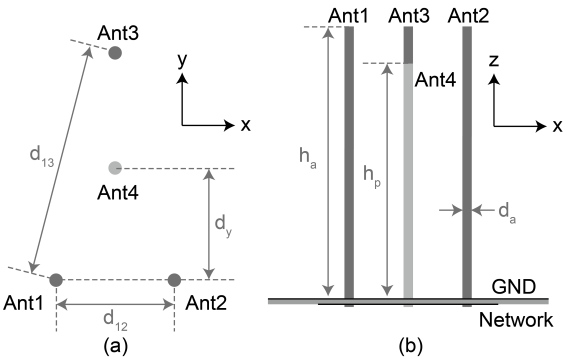

FIGURE 3. Configuration diagram of an isosceles triangular array with a loaded parasitic element on the axis. (a) Top view and (b) front view.

(4) Implement the load terminated at port 4.
(5) Implement the matching network for Y^G.
(6) Calculate the admittance parameters at plane t_2 by (13), and implement the neutralization section by (20) and (21).

III. DESIGN EXAMPLE AND GUIDELINES

In order to verify the proposed decoupling method, an isosceles triangular array consisting of three monopole antennas operating at 2.5 GHz is studied. The monopoles, brass rods with the same diameter d_a=1.12 mm and height h_a=28.6 mm, are implemented on a 120×120 mm^2 ground plane. The base elements (Ant1 and 2) are separated by d_{12}=12 mm=0.1λ, and the distance between the vertex element (Ant3) and Ant1/2 is d_{13}=d_{23}=24 mm=0.2λ, as depicted in Fig. 3. The selection of distances is to highlight the decoupling capability of the method proposed in this paper. In order to show that the applicability of this method is wider than [18], the side of the isosceles triangle differs from the base by 50%, which makes the isolations between the elements have a large difference.

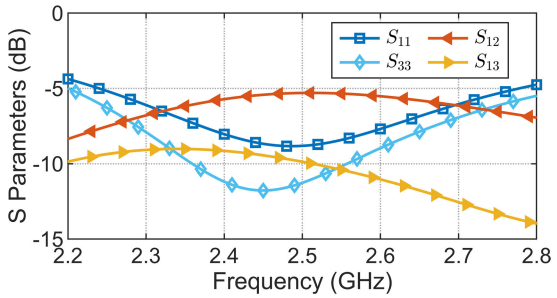

FIGURE 4. Simulated S parameters of the coupled array.

The simulated S-parameters of this three-port coupled array are given in Fig.4. The isolation between Ant1 and Ant2 is only 5.5 dB, and that between Ant3 and Ant1/2 is 10 dB. Apparently, the closer the distance between two elements, the stronger their mutual coupling.

As described in Section II, the decoupling is performed as follows.

Step (1) to (3):

A loaded parasitic element (Ant 4) is then introduced on the axis. The distance from Ant4 to the base is denoted by d_y. At each position of Ant4 inside the triangle, the length of the monopole and the load value can be obtained to eliminate the coupling between Ant3 and Ant1/2. Then the corresponding Y^B can be calculated by (8), and the design parameters of the ITS are obtained by (16) and (17).

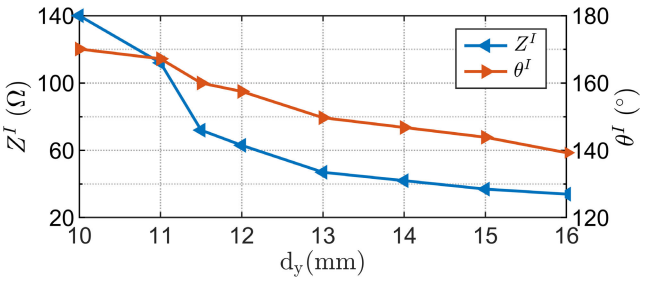

FIGURE 5. Parameters of the ITS with different positions of the LPE by EM simulations.

Fig. 5 shows the simulated parameters of the ITS in case of different positions with the step of 1mm. There exist two sets of solutions to the ITS, and one of them is omitted for its impracticable low impedance. We can observe that the TL's characteristic impedance and electrical length decrease with the d_y. The decoupling network is etched on an F4B substrate (ε_r = 2.6, tanδ = 0.002) with a thickness of 0.8 mm. Under the consideration of the machining error and layout, the line width will be proper when the line impedance varies from 35 Ω to 150 Ω. Although a shorter TL can be chosen, the reduction of the line length cannot offset the layout difficulties caused by the increase of the line width. Thus, the d_y with value between 11mm and 12mm may be proper.

The d_y of 11.5 mm is selected, and the length of the LPE is determined as h_p = 25.54 mm by EM sweeping. The admittance matrix of this four-element array is calculated by ANSYS HFSS as (22), shown at the bottom of the next page.

Then Y_L calculated by (5) is $-j34.41$ mS, and Y^G calculated by (6) is $30.64e^{-j65.1^\circ}$ mS. $\boldsymbol{Y^B}$ can be derived by (8) as

$$\boldsymbol{Y^B} = \begin{bmatrix} 12.49 - j41.97 & 3.92 + j29.19 \\ 3.92 + j29.19 & 12.49 - j41.97 \end{bmatrix} mS \quad (23)$$

The corresponding parameters of the ITS are derived as $Z^I = 72\ \Omega$ and $\theta^I = 160^\circ$ by (16) and (17).

Step (4):

The load of the parasitic element calculated through (5) is $Y_L = -j34.41$ mS, which can be implemented by a shorted stub of Z_L = 54 Ω and θ_L = 28.4°. The length of a shorted stub cannot be adjusted like an open stub, so the susceptance loaded can be modified easily using a larger width corresponding to a low impedance.

Step (5):

In Fig. 6, it can be seen that the isolation between Ant3 and Ant1/2 is raised to more than 40 dB at the center frequency by the LPE. As a result, the cascading ITSs to Ant1 and 2 has almost no effect on Ant3. The admittance of Ant3 remains $Y^G = 12.9 - j22.79$ mS, which can be matched by a shunted

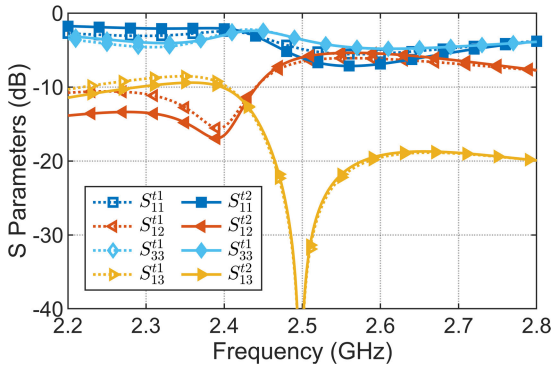

FIGURE 6. Simulated S parameter. Dotted lines denote the case introducing the LPE, and the case cascaded by a pair of ITSs additionally is represented by solid lines.

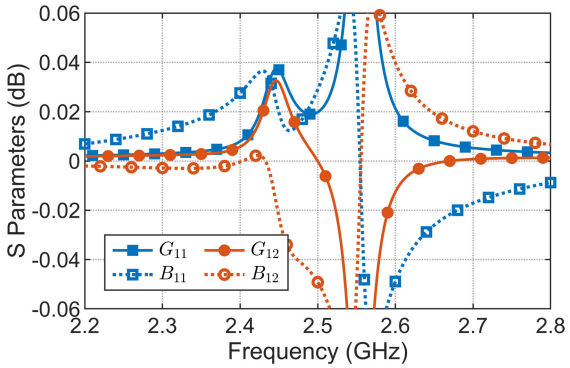

FIGURE 7. Simulated Y parameters at t_2.

open stub of $Z = 75\ \Omega$ and $\theta = 64.1°$, and a cascaded $\lambda/4$ TL of $Z = 62\ \Omega$.

Step (6):

The effect of ITSs on the admittance transforming is verified in Fig. 7. At the reference plane t_2, the self- and trans-conductives calculated by (13) are converted to the source admittance and zero at the center frequency, respectively.

The remained self-susceptance is 29 mS, and the trans-susceptance is -49.2 mS. Thus, the design parameters of the NS can be calculated by (20) and (21). The impedance and the electrical length of the main line are determined by (20), a single equation. Because the value of the trans-susceptance to be compensated is small, a low impedance of 50 Ω is chosen to get a slightly longer electrical length of 24°. Then the loads attached to the two ends of the main line is calculated to be $Y_L = -j15.8$ mS, which is realized by an open stub of $Z^I = 75\ \Omega$ and $\theta^I = 49.8°$.

The parameters of the decoupling and matching networks are annotated in Fig. 8 and summarized in TABLE 1. To simplify the annotations, lengths of all the TLs are measured at the center points of the cross-sections. The slight differences between the theoretical values and sizes of TLs are caused by the discontinuities.

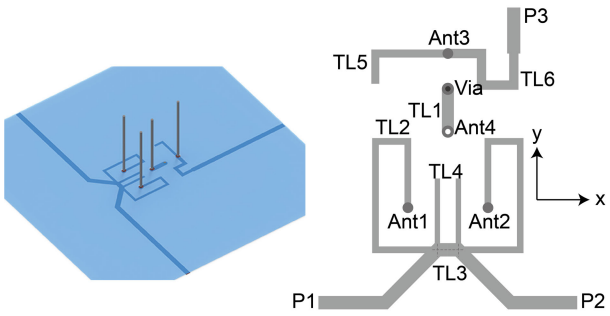

FIGURE 8. Diagram of the networks etched on the substrate.

TABLE 1. Parameters and dimensions of the networks.

TL	Z (Ω)	θ (deg)	Width (mm)	Length (mm)
1	54	28.4	2	6.48
2	72	160	1.2	10+5+16.39+9.43
3	50	24	2.2	3.15
4	75	49.8	1.12	10.88
5	75	64.1	1.12	11+4.61
6	62	90	1.35	5+4.9+5+4.9

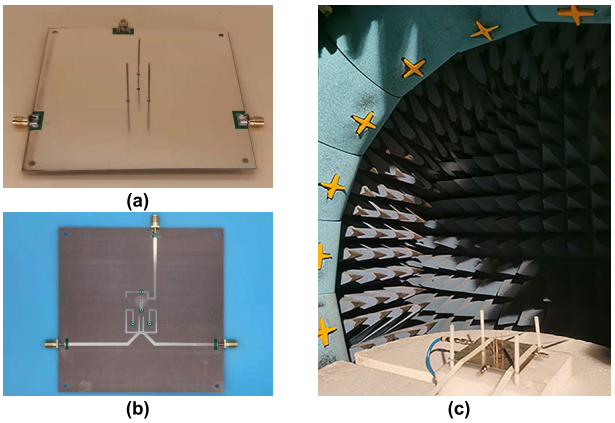

FIGURE 9. The fabricated (a) decoupled array with (b) the decoupling and matching networks; (c) the measurement of the radiation pattern.

IV. MEASUREMENT RESULTS AND DISCUSSION

The fabricated decoupled array and its measurement of the radiation pattern are given in Fig. 9. The simulated and measured S parameters are given in Fig. 10, which verify the effectiveness of the proposed method. The decoupling and matching of an antenna array, is the diagonalization and normalization of the admittance matrix, which is a process

$$\boldsymbol{Y^A} = \begin{bmatrix} 35.82e^{-j70.4°} & 37.64e^{j96.7°} & 14.71e^{j91.5°} & 12.04e^{-j88.7°} \\ 37.64e^{j96.7°} & 35.82e^{-j70.4°} & 14.71e^{j91.5°} & 12.04e^{-j88.7°} \\ 14.71e^{j91.5°} & 14.71e^{j91.5°} & 13.16e^{-j8.2°} & 21.22e^{-j90.5°} \\ 12.04e^{-j88.7°} & 12.04e^{-j88.7°} & 21.22e^{-j90.5°} & 51.79e^{j89.7°} \end{bmatrix} mS \tag{22}$$

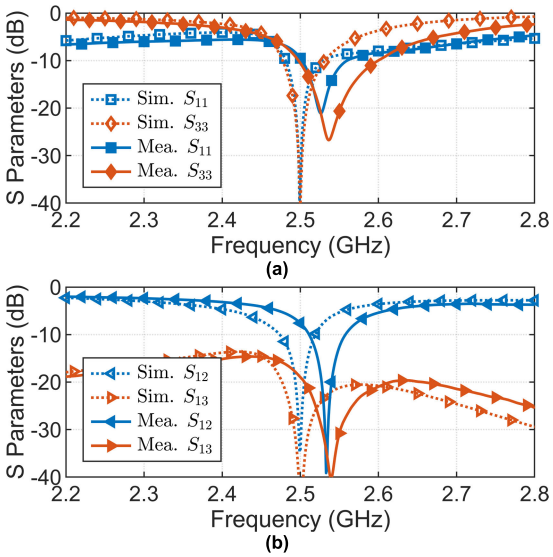

FIGURE 10. Simulated and Measured S parameters of the decoupled antenna array. (a) self-parameters and (b) trans-parameters.

of the admittance transformation of the matrix entries. Consequently, the conditions of decoupling and matching of an array with spacing of 0.1 λ and 0.2 λ can only be satisfied in a narrow band by the basic decoupling method with simple structures. The closer the distance between parallel monopoles, the larger the mutual coupling. Thus, the bandwidth of the decoupling between port 1 and port 2 is less than that between port 1 and port 3. The bandwidth of the decoupling can be expanded by deploying a wideband parasitic element and a second order decoupling and matching network.

The measured isolations are raised to about 35 dB and 40 dB at the center frequency where the return losses are greater than 20 dB, respectively. Although the center frequencies of the measured results shift towards high frequencies, the trend with the frequency is the same as the simulated results. The monopoles are pieces of metal wire welded to the dielectric board. The frequency deviations are the result of a decrease in the dielectric constant and the monopole length being shorter than the rated value caused by cutting and welding.

The radiation patterns of the simulated and measured decoupled array are given in Fig. 11. When Ant3 on the axis is excited, the direction of the main beam on the xoy plane is 90°. The pattern of port 2 is symmetrical to that of port 1, and it is not given for the sake of brevity. When Ant1 or Ant2 on the base is excited, the direction of the main beam is 220° or 320°, symmetrically. This feature of different maximum beam directions is required for applications involved multi-beam antennas. The monopoles are pieces of metal wire that are not perfectly straight and not welded strictly perpendicular to the substrate. Additionally, the substrate is slightly warped. The current distribution differs from that predicted by the simulation model. This results in ripples in the measured cross-polarization, which can be rectified by improving the accuracy of the fabrication and implement.

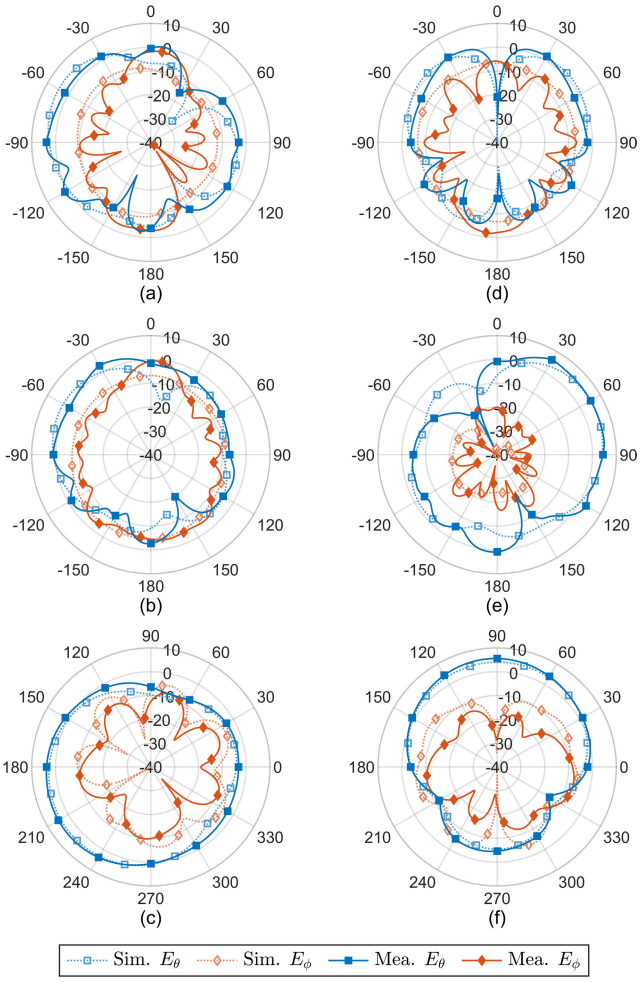

FIGURE 11. Simulated and measured radiation patterns of the proposed array: (a) $\phi = 0°$, (b) $\phi = 90°$, (c) $\theta = 90°$ with port 1 excited; (d) $\phi = 0°$, (e) $\phi = 90°$, (f) $\theta = 90°$ with port 3 excited.

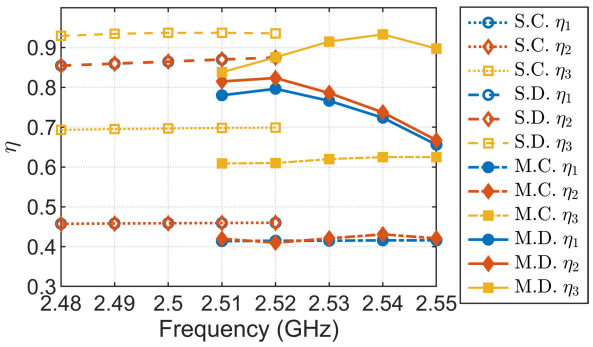

FIGURE 12. Simulated and measured efficiencies. (S., M., C., D., are shorted for simulated, measured, coupled and decoupled, respectively.)

The simulated and measured efficiencies around their own center frequencies of the array are shown in Fig. 12. The measured efficiencies of the decoupled base elements are greater than 70%, and that of the decoupled vertex element is about 85%. Each maximum value occurs at the frequency where the corresponding return loss is the largest. Various factors contribute to deviations between simulation results

TABLE 2. Comparison of the proposed decoupled three-element array with some existing arrays.

#	Type of Three-Element Array	Configuration Limited	Optimization Needed	# of Parasitic Element	Isolation (dB) Coupled	Decoupled	Enhancement
[31]	Equilateral triangle	–	–	0	9	20	11
[15]	Equilateral triangle	–	–	1	7.5	38	31.5
[29]	Line	✓	–	0	7.5/16	33/40+	25.5/24+
[17]	Line	–	✓	2	6.5/13.5	32/40	25.5/26.5
[18]	Isosceles triangle	✓	✓	1	9/11.5	32.5/39	23.5/27.5
[19]	Isosceles triangle	–	–	3	8/13	24/28	16/15
Proposed	Isosceles triangle	–	–	1	5/10	35/40	30

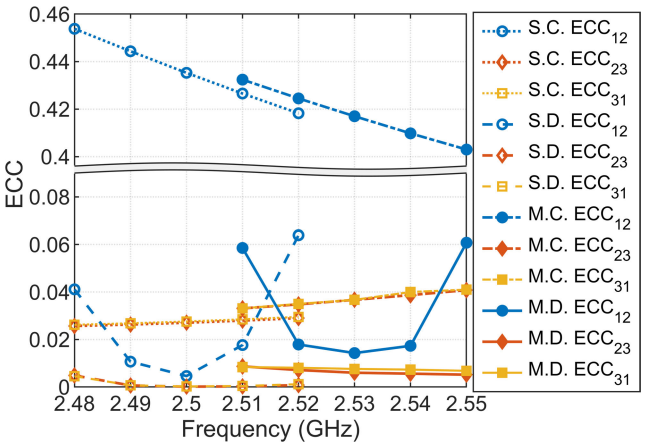

FIGURE 13. Simulated and measured efficiencies. (S., M., C., D., are shorted for simulated, measured, coupled and decoupled, respectively.)

and test results, including roughness of the metal surface, assembly error of monopoles, and measurement system error.

The envelope correlation coefficient (ECC) is a vital feature of the MIMO performance [32], which can be derived from the complex far-field radiation patterns as

$$\rho_{ij} = \frac{\int \left|\bar{E}_i(\theta,\phi)\cdot\bar{E}_j^*(\theta,\phi)\right|^2 d\Omega}{\int \left|\bar{E}_i(\theta,\phi)\right|^2 d\Omega \cdot \int \left|\bar{E}_j(\theta,\phi)\right|^2 d\Omega} \tag{24}$$

The simulated and measured ECCs of the array are shown in Fig. 13. The measured decoupled ECCs between Ant3 and Ant1/2 of the coupled array are reduced to 0.01, and the ECC between base elements is below 0.02 around the center frequency.

The decoupling results of three-element arrays in recent years are compared in TABLE 2. The method loaded with a single parasitic element [15] is very effective in dealing with equilateral triangular arrays, which can be extended to the isosceles triangular arrays where the mutual couplings between three elements are not much different (9 dB, 11.5 dB) [18]. When the vertex angle of the isosceles triangle has a more significant deviation from 60°, leading to a more considerable difference in mutual couplings, such as 5 dB in [19] and this paper, the method in [15] is not applicable. The method presented in this paper has no restrictions on the layout of the antenna, nor does it involve time-consuming EM optimizations. In addition, parasitic elements are reduced to one in this article compared with [19], and the decoupling effect achieved is first-class.

V. CONCLUSION

This paper proposes a hybrid LPE–DMN decoupling technique for closely spaced isosceles triangular arrays. The derived design formulas of the DMN provide direct insight into mechanisms of both impedance transforming and neutralization sections. Thus, we can take into account the parameters of the ITS while introducing the parasitic element.

In addition, instead of loading a stub at the center, we attach two stubs to two ends of a transmission line as the NS. As a result, compensating the trans-susceptance only depends on the parameters of the main line, which further facilitates the neutralization. The measured results show that sound isolation of 35 dB and return loss of 21 dB are obtained with ECCs less than 0.02, which validate this decoupling strategy of overall planning and dividing and conquering. It is suitable for various types of antennas and can be extended to the decoupling of scalene triangle arrays. Moreover, the proposed π-shaped transmission line is a good candidate for the DMNs.

REFERENCES

[1] J. W. Wallace, M. A. Jensen, A. L. Swindlehurst, and B. D. Jeffs, "Experimental characterization of the MIMO wireless channel: Data acquisition and analysis," *IEEE Trans. Wireless Commun.*, vol. 2, no. 2, pp. 335–343, Mar. 2003.

[2] R. W. Heath and A. Lozano, *Foundations of MIMO Communication*. Cambridge, U.K.: Cambridge Univ. Press, 2018.

[3] W. K. Kahn, "Ideal efficiency of a radiating element in an infinite array," *IEEE Trans. Antennas Propag.*, vol. AP-15, no. 4, pp. 534–538, Jul. 1967.

[4] X. Tang, K. Mouthaan, and J. C. Coetzee, "Tunable decoupling and matching network for diversity enhancement of closely spaced antennas," *IEEE Antennas Wireless Propag. Lett.*, vol. 11, pp. 268–271, 2012.

[5] D. Sievenpiper, L. Zhang, R. F. J. Broas, N. G. Alexopolous, and E. Yablonovitch, "High-impedance electromagnetic surfaces with a forbidden frequency band," *IEEE Trans. Microw. Theory Techn.*, vol. 47, no. 11, pp. 2059–2074, Nov. 1999.

[6] F. Yang and Y. Rahmat-Samii, "Microstrip antennas integrated with electromagnetic band-gap (EBG) structures: A low mutual coupling design for array applications," *IEEE Trans. Antennas Propag.*, vol. 51, no. 10, pp. 2936–2946, Oct. 2003.

[7] J. Y. Deng, J. Li, L. Zhao, and L. Guo, "A dual-band inverted-F MIMO antenna with enhanced isolation for WLAN applications," *IEEE Antennas Wireless Propag. Lett.*, vol. 16, pp. 2270–2273, Jun. 2017.

[8] M. Karaboikis, C. Soras, G. Tsachtsiris, and V. Makios, "Compact dual-printed inverted-F antenna diversity systems for portable wireless devices," *IEEE Antennas Wireless Propag. Lett.*, vol. 3, no. 1, pp. 9–14, Dec. 2004.

[9] T.-Y. Wu, S.-T. Fang, and K.-L. Wong, "Printed diversity monopole antenna for WLAN operation," *Electron. Lett.*, vol. 38, no. 25, pp. 1625–1626, Dec. 2002.

[10] A. C. K. Mak, C. R. Rowell, and R. D. Murch, "Isolation enhancement between two closely packed antennas," *IEEE Trans. Antennas Propag.*, vol. 56, no. 11, pp. 3411–3419, Nov. 2008.

[11] Y. Liu, Y. Wang, and Z. Du, "A broadband dual-antenna system operating at the WLAN/WiMax bands for laptop computers," *IEEE Antennas Wireless Propag. Lett.*, vol. 14, pp. 1060–1063, 2015.

[12] J.-N. Hwang and S.-J. Chung, "Isolation enhancement between two packed antennas with coupling element," *IEEE Antennas Wireless Propag. Lett.*, vol. 10, pp. 1263–1266, 2011.
[13] A. Diallo, C. Luxey, P. Le Thuc, R. Staraj, and G. Kossiavas, "Study and reduction of the mutual coupling between two mobile phone PIFAs operating in the DCS1800 and UMTS bands," *IEEE Trans. Antennas Propag.*, vol. 54, no. 11, pp. 3063–3074, Nov. 2006.
[14] S.-W. Su, C.-T. Lee, and F.-S. Chang, "Printed MIMO-antenna system using neutralization-line technique for wireless USB-dongle applications," *IEEE Trans. Antennas Propag.*, vol. 60, no. 2, pp. 456–463, Feb. 2012.
[15] B. K. Lau and J. B. Andersen, "Simple and efficient decoupling of compact arrays with parasitic scatterers," *IEEE Trans. Antennas Propag.*, vol. 60, no. 2, pp. 464–472, Feb. 2012.
[16] L. Zhao and K.-L. Wu, "A decoupling technique for four-element symmetric arrays with reactively loaded dummy elements," *IEEE Trans. Antennas Propag.*, vol. 62, no. 8, pp. 4416–4421, Aug. 2014.
[17] J.-Y. Deng, J.-Y. Li, and L.-X. Guo, "Decoupling of a three-port MIMO antenna with different impedances using reactively loaded dummy elements," *IEEE Antennas Wireless Propag. Lett.*, vol. 17, no. 3, pp. 430–433, Mar. 2018.
[18] L. Zhao and K.-L. Wu, "Decoupling of an isosceles triangular three element array with one reactively loaded dummy element," in *IEEE MTT-S Int. Microw. Symp. Dig.*, Jun. 2014, pp. 1–3.
[19] M. Li, D. Wu, B. Xiao, K. L. Yeung, and L. Jiang, "A novel calculation method to design parasitic decoupling technique for two antennas," *IEEE Access*, vol. 8, pp. 116041–116051, 2020.
[20] T.-I. Lee and Y. E. Wang, "Mode-based information channels in closely coupled dipole pairs," *IEEE Trans. Antennas Propag.*, vol. 56, no. 12, pp. 3804–3811, Dec. 2008.
[21] C. Volmer, J. Weber, R. Stephan, K. Blau, and M. A. Hein, "An Eigen-analysis of compact antenna arrays and its application to port decoupling," *IEEE Trans. Antennas Propag.*, vol. 56, no. 2, pp. 360–370, Feb. 2008.
[22] S. C. Chen, Y. S. Wang, and S. J. Chung, "A decoupling technique for increasing the port isolation between two strongly coupled antennas," *IEEE Trans. Antennas Propag.*, vol. 56, no. 12, pp. 3650–3658, Dec. 2008.
[23] X. Tang, K. Mouthaan, and J. C. Coetzee, "Flexible design of decoupling and matching networks for two strongly coupled antennas," *Electron. Lett.*, vol. 49, no. 8, pp. 521–522, Apr. 2013.
[24] J. C. Coetzee and Y. Yu, "Closed-form design equations for decoupling networks of small arrays," *Electron. Lett.*, vol. 44, no. 25, p. 1441, 2008.
[25] C.-H. Wu, G.-T. Zhou, Y.-L. Wu, and T.-G. Ma, "Stub-loaded reactive decoupling network for two-element array using even–odd analysis," *IEEE Antennas Wireless Propag. Lett.*, vol. 12, pp. 452–455, 2013.
[26] L. Zhao, L. K. Yeung, and K.-L. Wu, "A coupled resonator decoupling network for two-element compact antenna arrays in mobile terminals," *IEEE Trans. Antennas Propag.*, vol. 62, no. 5, pp. 2767–2776, May 2014.
[27] L. Zhao and K.-L. Wu, "A broadband coupled resonator decoupling network for a three-element compact array," in *IEEE MTT-S Int. Microw. Symp. Dig.*, Jun. 2013, pp. 1–3.
[28] Y.-F. Cheng and K.-K. M. Cheng, "A novel and simple decoupling method for a three-element antenna array," *IEEE Antennas Wireless Propag. Lett.*, vol. 16, pp. 1072–1075, 2017.
[29] H. J. Chaloupka, X. Wang, and J. C. Coetzee, "A superdirective 3-element array for adaptive beamforming," *Microw. Opt. Technol. Lett.*, vol. 36, no. 6, pp. 425–430, Mar. 2003.
[30] J. Kornprobst, T. J. Mittermaier, R. A. M. Mauermayer, G. F. Hamberger, M. G. Ehrnsperger, B. Lehmeyer, M. T. Ivrlac, U. Imberg, T. F. Eibert, and J. A. Nossek, "Compact uniform circular quarter-wavelength monopole antenna arrays with wideband decoupling and matching networks," *IEEE Trans. Antennas Propag.*, vol. 69, no. 2, pp. 769–783, Feb. 2021.
[31] R. G. Vaughan and J. B. Andersen, "Antenna diversity in mobile communications," *IEEE Trans. Veh. Technol.*, vol. VT-36, no. 4, pp. 149–172, Nov. 1987.

CHI ZHANG (Member, IEEE) received the B.S. degree from Xidian University, Xi'an, China, in 2012, where he is currently pursuing the Ph.D. degree. His current research interests include antenna decoupling techniques and microwave passive circuits.

YONG-CHANG JIAO (Senior Member, IEEE) received the Ph.D. degree in electrical engineering from Xidian University, Xi'an, China, in 1990. In 1990, he joined the Institute of Antennas and EM Scattering, Xidian University, where he is currently a Professor. From March to June in 1996, he was a JSPS Visiting Priority-Area Research Fellow with the University of Tsukuba, Tsukuba, Japan. From March to September in 2002, he was a Research Fellow with the City University of Hong Kong, Hong Kong. He has authored or coauthored over 300 papers in technical journals and conference proceedings. His papers have been cited more than 2700 times with an H-index is 29 (source: ISI Web of Science). His current research interests include antenna designs, computational electromagnetics, and microwave passive components. He is a Senior Member of the Chinese Institute of Electronics (CIE) and a member of the Antenna Committee of CIE.

JINGXUAN WEN received the B.S. degree from Xidian University, Xi'an, China, in 2018, where he is currently pursuing the M.S. degree with the Department of National Key Laboratory of Antennas and Microwave Technology. His current research interests include high-gain antennas and 5G MMW antenna techniques.

YANG-DONG YAN received the B.S. and M.S. degrees from Xidian University, Xi'an, China, in 2006 and 2010, respectively, where he is currently pursuing the Ph.D. degree in electromagnetics and microwave technology with the Department of National Key Laboratory of Antennas and Microwave Technology. His current research interests include RF, EMC/EMI, antennas and phased arrays, and 5G communication technology.

ZIBIN WENG (Senior Member, IEEE) received the B.S. degree in electronic engineering and the Ph.D. degree in electromagnetic field and microwave technology from Xidian University, Xi'an, China, in 2004 and 2009, respectively. He is currently an Associate Professor with Xidian University. His current research interests include circularly polarized antennas, millimeter-wave antennas, and antenna arrays.